mathematics

Article

On Generalized Fourier's and Fick's Laws in Bio-Convection Flow of Magnetized Burgers' Nanofluid Utilizing Motile Microorganisms

Ali Saleh Alshomrani

Department of Mathematics, Faculty of Science, King Abdulaziz University, Jeddah 21589, Saudi Arabia; aszalshomrani@kau.edu.sa

Received: 6 July 2020; Accepted: 17 July 2020; Published: 19 July 2020

Abstract: This article describes the features of bio-convection and motile microorganisms in magnetized Burgers' nanoliquid flows by stretchable sheet. Theory of Cattaneo–Christov mass and heat diffusions is also discussed. The Buongiorno phenomenon for nanoliquid motion in a Burgers' fluid is employed in view of the Cattaneo–Christov relation. The control structure of governing partial differential equations (PDEs) is changed into appropriate ordinary differential equations (ODEs) by suitable transformations. To get numerical results of nonlinear systems, the bvp4c solver provided in the commercial software MATLAB is employed. Numerical and graphical data for velocity, temperature, nanoparticles concentration and microorganism profiles are obtained by considering various estimations of prominent physical parameters. Our computations depict that the temperature field has direct relation with the thermal Biot number and Burgers' fluid parameter. Here, temperature field is enhanced for growing estimations of thermal Biot number and Burgers' fluid parameter.

Keywords: Burgers' nanofluid; heat generation/absorption; bio-convection; Cattaneo–Christov relations; motile microorganisms; numerical solution

1. Introduction

Nowadays investigators are showing huge interest in nanofluid heat transfer applications. Based on the empirical results, working fluids in various technical and medical fields have been found to have the robust features of heat transfer, mass and density during the flow. While different base liquids have similar heat transfer capability, due to poor thermal efficiency, such liquids are typically not favored for heat transport applications. In order to overcome this problem, heat efficiency of such conventional techniques can be boosted by the usage of some nanoparticles additives. Suspension of regular fluids with nano-size materials is deemed to become most efficient solution to enhance heat transport that has been used in a wide range of products in different air-conditioning systems. With this concept, convectional fluids with lower heat efficiency have been substituted by nanoliquids that are capable of transmitting further heat to devices. Compared to ordinary fluids, nanoliquids are generally extra stable in terms of heat and momentum transfer. Such nanomaterials can be enhanced by utilizing different metals such as gold, silver, copper, steel, borides, oxides and nitrides with special caution.

Choi [1] introduced the term "nanofluid". Buongiorno [2] analyzed the concept of natural convective transport in a nanofluid. Many researchers have studied the nature of the nanofluid flow via Brownian motion and thermophoretic factors. Turkyilmazoglu [3] researched the influence of single-phase nanoliquids and its linear stabilization. Ellahi et al. [4] studied nano-sized hafnium particles. The results of second-order slip over a Poiseuille nanoliquid flow subject to the impact of Stefan blows in channels were identified by Alamri et al. [5]. Khan et al. [6] analyzed the conservation-based performance evaluation of hybrid nanoliquid-assisted composite materials. Irfan et al. [7] researched the movement of EMHD nanoliquids over fixed thickness sheets. Reddy et al. [8] analyzed the movement of chemically reacting stagnation point Powell-Eyring nanoliquids flowing through an inclined cylinder subject to energy activation and Cattaneo–Christov heat transfer. Khan et al. [9] observed the behavior of nonlinear heat radiation by using nanomaterials and activation energy. Agamid et al. [10] discussed the unsteady flow of carbon nanotubes based-fluids between two moving disks. Uddin et al. [11] addressed the actions of nanomaterials to disperse blood across a cylindrical tube utilizing a single kernel. Abbas et al. [12] investigated the non-uniform hemodynamic nanoliquid motion. Babazadeh et al. [13] discussed the process of modifying Lorentz's force over nanoparticles flowing inside two disks. Alamri et al. [14] examined the impact of mass transport on the second-grade liquid movement. Niazmand et al. [15] discussed the impact of nanoparticles in a lamp-driven cylindrical cavity. Steady 2D convective viscous nanoliquid flow by a stretchable cylinder with a chemical process was explored by Mondal et al. [16]. Saif et al. [17] addressed hydromagnetic Jeffrey nanoliquid flow through a curved stretched surface. Nanoliquid turbulence and flow in an annular space was studied mathematically and experimentally by Abdulrazzaq et al. [18]. Saeed et al. [19] analyzed the transport of heat through a porous stretched cylinder and Darcy-Forchheimer hybrid-nanoliquid movement. Souayeh et al. [20] examined radiative heat transition and slippery flow through nanofluid. Tlili et al. [21] studied boundary-layer MHD flow subject to convection features across a wedge. Farhangmehr et al. [22] numerically investigated the MHD flow of a nanofluid over a moving surface. Many researchers have worked on nanofluids as may be seen in various publications [23–30].

The occurrence of bioconvection is correlated with microorganisms and biological solutions. Such a practice is generally noted in dilute liquids in which microorganisms travel upward in a suspended liquid resulting in instability due to concentration stratification. The bioconvection mechanism is understood by Rayleigh-Bernard convection which is also visible in the reversal of the nanofluid instability caused by the haphazard motion of nanomaterials. The key difference between molecules and a biological suspension is that nanomaterials are not self-propelled and they follow Brownian motion owing to hydrodynamic instability. Introduction of swimming gyrotactic motile microorganisms into a nanoliquid is known to cause a significant change in the fluid convection behavior. Kuznetsov and Avramenko [31] have introduced the bioconvection of nanomaterials through a horizontal convection sheet in the occurrence of swimming microorganisms. Ghorai and Hill [32] additionally clarified that bioconvection can be utilized to illustrate the process of impulsive model improvement in fluids containing microorganisms like bacteria and algae. Atif et al. [33] scrutinized the homogenous micropolar bioconvective fluid flow with nanoparticles and gyrotactic microorganisms. Khan et al. [34] inspected 2D bioconvection coupled stress fluid flow with nanoparticles, magnetic field and gyrotactic motile microorganisms. Amirsom et al. [35] presented theoretical research on the 3D movement of bioconvection nanoliquids comprising gyrotactic motile microorganisms throughout a bi-axial stretched sheet. Zhang et al. [36] determined the features of activation energy in radiative rate-type nanofluid with bioconvection aspect configured by stretching/shrinking disks. Usman et al. [37] studied the model of three-dimensional nanoliquid bioconvection with a stagnation connection. Basir et al. [38] proposed nanoliquid laminar convective MHD flow through heat, mass and gyrotactic microorganism transfers. The bioconvection motion of a Carreau nanofluid over a wedge was addressed by Muhammad et al. [39]. Mansour et al. [40] presented a mathematical analysis of magneto-hydrodynamic convective flow with gyrotactic motile microorganisms in a squared lid-driven space. Li et al. [41] investigated the bioconvection flow of generalized second grade nanofluids under the effect of Wu's slip. Waqas et al. [42] scrutinized the non-thermal radiation behavior in Oldroyd-B nanofluid flow with swimming motile microorganisms past a rotating disk. More works on bioconvection can be found in [43–50].

The objective of the present research article is to explore the bio-convection flow of a magnetized Burgers' nanofluid subject to the presence of swimming motile microorganisms. The Buongiorno expressions for nanoliquid motion in the Burgers' fluid are employed in view of generalized Fourier's and Fick's laws. Partial differential equations (PDEs) are changed into appropriate ordinary differential equations (ODEs) by suitable transformations [51–54]. To perform numerical computations of nonlinear expressions, the bvp4c solver in the commercial software MATLAB is employed. Numerical and graphical results for velocity, nanofluid temperature, nanofluid concentration, microorganisms, skin friction, Nusselt, Sherwood and motile density numbers are obtained by considering various estimations of physical numbers.

2. Mathematical Formulation

A mathematical relation is designed for 2D Burgers nanofluid flow with Cattaneo–Christov models, motile microorganisms and bioconvection past a stretching sheet. Impacts of Brownian movement and thermophoresis diffusion are also taken into account. Furthermore, stagnation point flow and thermal and solutal stratifications are scrutinized. Wall temperature of nanoparticles (T_w), wall concentration of nanoparticles (C_w) and wall motile microorganisms (N_w) are considered. Moreover, (T_∞) is the ambient temperature, (C_∞) is the ambient concentration and (N_∞) is the ambient microorganism. The velocity components are associated in the way of x-axis and y-axis which are depicted in Figure 1.

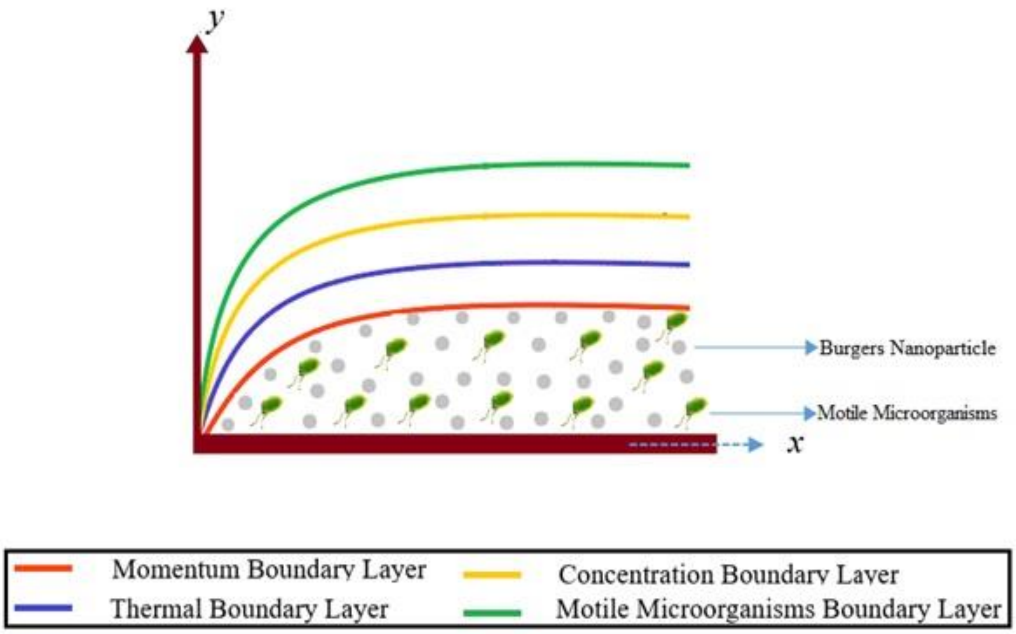

Figure 1. Flow model of the problem.

The rate-type liquid expressed via a Burgers' liquid is:

$$\left(1+\lambda_1\frac{D}{Dt}+\lambda_2\frac{D^2}{Dt^2}\right)S=\mu\left(1+\lambda_3\frac{D}{Dt}\right)A_1 \tag{1}$$

Here (S) stands for extra stress tensor, (μ) for the dynamic viscosity of the fluid, $\left(A_1=(\nabla.V)+(\nabla.V)^T\right)$ for the first Rivilin-Ericksen tensor and $\left(\frac{D}{Dt}\right)$ for the upper convective derivative. The continuity and momentum expressions for present flow are:

$$\nabla.V=0, \tag{2}$$

$$\rho_f\frac{dV}{d}t=-\nabla p+divS+J_1\times B, \tag{3}$$

where the energy law conservation for the present model is:

$$\left(\rho C_p\right)\frac{dT}{dt}-\left(\rho C_p\right)\left[D_B\nabla C.\nabla T+\frac{D_T}{D_\infty}(\nabla T)^2\right]=-\nabla.q+Q_0(T-T_\infty), \tag{4}$$

in which (q) stands for heat flux satisfy the following property:

$$q+\lambda_1\left[\frac{\partial q}{\partial t}+V.\nabla q-q.\nabla V+(\nabla.V)q\right]=-k\nabla T, \tag{5}$$

where the nanoparticles concentration for the present flow model is:

$$\frac{dC}{dt}-\frac{D_T}{D_\infty}\nabla^2T=-\nabla.J-k_c(C-C_\infty), \tag{6}$$

in which (J) stands for the mass flux satisfying the following property:

$$J+\lambda_c\left[\frac{\partial J}{\partial t}+V.\nabla J-J.\nabla V+(\nabla.V)J\right]=D_B\nabla C. \tag{7}$$

Here (ν) stands for kinematic viscosity, (λ_1) for the fluid relaxation time, (λ_2) for material parameter of the Burgers' fluid, $(\lambda_3\leq\lambda_1)$ for the fluid retardation time, (λ_c) for the mass relaxation time, (λ_t) for the thermal relaxation time, (T) for the liquid temperature, (C) for the liquid concentration, (T_∞) for the ambient temperature, (C_∞) for the ambient concentration, (D_B) for the diffusion coefficient, (J_1) for the current density, (q) for the heat flux and (J) for the mass flux. The governing expressions for the current flow model are:

$$\frac{\partial u}{\partial x}+\frac{\partial v}{\partial y}=0, \tag{8}$$

$$\begin{aligned}
&u\tfrac{\partial u}{\partial x}+v\tfrac{\partial v}{\partial y}+\lambda_1\left[u^2\tfrac{\partial^2u}{\partial x^2}+v^2\tfrac{\partial^2v}{\partial y^2}+2uvv\tfrac{\partial^2u}{\partial x\partial y}\right]\\
&+\lambda_2\left[\begin{array}{l}u^3\tfrac{\partial^3u}{\partial x^3}+v^3\tfrac{\partial^3v}{\partial y^3}+u^2\left(\tfrac{\partial v}{\partial x}\tfrac{\partial^2u}{\partial x\partial y}-\tfrac{\partial u}{\partial x}\tfrac{\partial^2v}{\partial x^2}+\tfrac{\partial u}{\partial x}\tfrac{\partial^2u}{\partial x^2}\right)+3v^2\left(\tfrac{\partial v}{\partial y}\tfrac{\partial^2u}{\partial y^2}+\tfrac{\partial u}{\partial y}\tfrac{\partial^2u}{\partial x\partial y}\right)\\+3uv\left(u\tfrac{\partial^3u}{\partial x^2\partial y}+v\tfrac{\partial^3u}{\partial x\partial y^2}\right)+2uv\left(\tfrac{\partial v}{\partial y}\tfrac{\partial^2u}{\partial x\partial y}+\tfrac{\partial v}{\partial x}\tfrac{\partial^2u}{\partial y^2}+\tfrac{\partial u}{\partial y}\tfrac{\partial^2u}{\partial x^2}-\tfrac{\partial u}{\partial y}\tfrac{\partial^2v}{\partial x\partial y}\right)\end{array}\right]\\
&=v\lambda_3\left[v\tfrac{\partial^3v}{\partial y^3}+u\tfrac{\partial^3u}{\partial x\partial y^2}-\tfrac{\partial u}{\partial x}\tfrac{\partial^2u}{\partial y^2}-\tfrac{\partial u}{\partial y}\tfrac{\partial^2v}{\partial y^2}\right]+v\left[\tfrac{\partial^2u}{\partial y^2}\right]+\tfrac{dU_e}{dx}\\
&-\tfrac{\sigma B_0^2}{\rho}\left[u-U_e+\lambda_1v\tfrac{\partial u}{\partial y}+\lambda_2\left(u\tfrac{\partial v}{\partial x}\tfrac{\partial^2u}{\partial y^2}-v\tfrac{\partial u}{\partial x}\tfrac{\partial^2u}{\partial y^2}+uv\tfrac{\partial^2u}{\partial x\partial y}+v^2\tfrac{\partial^2u}{\partial y^2}\right)\right]\\
&+\tfrac{1}{\rho_f}\left[\begin{array}{l}\left(1-C_f\right)\rho_f\beta^{**}g^*(T-T_\infty)-\left(\rho_p-\rho_f\right)g^*(C-C_\infty)\\-(N-N_\infty)g^*\gamma\left(\rho_m-\rho_f\right)\end{array}\right],
\end{aligned} \tag{9}$$

$$\begin{aligned}
&u\tfrac{\partial T}{\partial x}+v\tfrac{\partial T}{\partial y}=\alpha\left(\tfrac{\partial^2T}{\partial y^2}\right)-\lambda_1\left[\begin{array}{l}u^2\tfrac{\partial^2T}{\partial x^2}+v^2\tfrac{\partial^2T}{\partial y^2}+2uvv\tfrac{\partial^2T}{\partial x\partial y}+\tfrac{\partial T}{\partial x}\left(u\tfrac{\partial u}{\partial x}+v\tfrac{\partial u}{\partial y}\right)\\+\tfrac{\partial T}{\partial y}\left(u\tfrac{\partial v}{\partial x}+v\tfrac{\partial v}{\partial y}\right)\end{array}\right]\\
&+\lambda^*{}_t\tau D_B\left[u\tfrac{\partial^2C}{\partial x\partial y}\tfrac{\partial T}{\partial y}+u\tfrac{\partial C}{\partial y}\tfrac{\partial^2T}{\partial x\partial y}+v\tfrac{\partial^2C}{\partial y^2}\tfrac{\partial T}{\partial y}+v\tfrac{\partial C}{\partial y}\tfrac{\partial^2T}{\partial y^2}\right]+2\lambda^*{}_t\tau\tfrac{D_T}{D_\infty}\left[\begin{array}{l}u\tfrac{\partial T}{\partial y}\tfrac{\partial^2T}{\partial x\partial y}\\+u\tfrac{\partial^2T}{\partial y^2}\tfrac{\partial T}{\partial y}\end{array}\right]\\
&+\tfrac{Q_0}{\rho C_p}(T-T_\infty)+\lambda^*{}_t\tfrac{Q_0}{\rho C_p}\left(v\tfrac{\partial T}{\partial y}+u\tfrac{\partial T}{\partial x}\right)+\tfrac{1}{(\rho c)_f}\tfrac{\partial}{\partial y}\left(\tfrac{16\sigma^*T_\infty^3}{3k^*}\left(\tfrac{\partial T}{\partial y}\right)\right)
\end{aligned} \tag{10}$$

$$\begin{aligned}
&u\tfrac{\partial C}{\partial x}+v\tfrac{\partial C}{\partial y}=D_B\left(\tfrac{\partial^2C}{\partial y^2}\right)-\lambda^*{}_c\left[\begin{array}{l}u^2\tfrac{\partial^2C}{\partial x^2}+v^2\tfrac{\partial^2C}{\partial y^2}+2uv\tfrac{\partial^2C}{\partial x\partial y}+\tfrac{\partial C}{\partial x}\left(u\tfrac{\partial u}{\partial x}+v\tfrac{\partial u}{\partial y}\right)\\+\tfrac{\partial C}{\partial y}\left(u\tfrac{\partial v}{\partial x}+v\tfrac{\partial v}{\partial y}\right)\end{array}\right]\\
&-\tfrac{D_T}{T_\infty}\left[u\tfrac{\partial^3T}{\partial x\partial y^2}+u\tfrac{\partial^3C}{\partial y^3}+\tfrac{\partial^2T}{\partial y^2}\right]-Kr^2(C-C_\infty)\left(\tfrac{T}{T_\infty}\right)^n\exp\left(\tfrac{-E_a}{kT}\right)-\lambda^*{}_ck_c\left(v\tfrac{\partial C}{\partial y}+u\tfrac{\partial C}{\partial x}\right),
\end{aligned} \tag{11}$$

$$u\frac{\partial N}{\partial x}+v\frac{\partial N}{\partial y}+\frac{bW_c}{(C_w-C_\infty)}\left[\frac{\partial}{\partial y}\left(N\frac{\partial C}{\partial y}\right)\right]=D_m\frac{\partial^2N}{\partial y^2}, \tag{12}$$

$$\begin{aligned} &u = U_w = cx,\ v = 0,\ \ -k\tfrac{\partial T}{\partial y} = h_f(T_w - T), -D_B\tfrac{\partial C}{\partial y} = h_g(C_w - C), \\ &-D_m\tfrac{\partial N}{\partial y} = h_n(N_w - N) \qquad\qquad at\ y = 0, \end{aligned} \tag{13}$$

$$v \to 0,\ \frac{\partial u}{\partial y} \to 0, T \to T_w, C \to C_w, N \to N_w\ as\ y \to \infty \tag{14}$$

Here $\left(\alpha = \frac{k}{\rho Cp}\right)$ stands for the thermal diffusivity, (ρ) for the density, (p) for the pressure, $\left(C_p\right)$ for the specific heat capacity and (k) for the liquid thermal conductivity. The appropriate transformations are expressed by:

$$\left.\begin{aligned} &\psi = x\sqrt{cv}f(\zeta), u = cxf'(\zeta),\ v = -\sqrt{cv}f(\zeta),\ \theta(\zeta) = \tfrac{T-T_\infty}{T_w-T_\infty}, \\ &\phi(\zeta) = \tfrac{C-C_\infty}{C_w-C_\infty},\ \chi(\zeta) = \tfrac{N-N_\infty}{N_w-N_\infty},\ \zeta = y\sqrt{\tfrac{c}{v}} \end{aligned}\right\}. \tag{15}$$

PDEs are altered to the following ODEs by utilizing the above transformations:

$$\begin{aligned} &f''' + ff'' - (f')^2 + \alpha_1\left[2ff'f'' - f^2f'''\right] - \alpha_2\left[3f^2(f'')^2 - 2f(f')^2f'' - f^3f^{iv}\right] \\ &+\alpha_3\left[(f'')^2 - ff^{iv}\right] - M^2[\alpha_2ff''' - \alpha_1ff'' + f'] + K^2 + M^2K + \lambda(\theta - Nr\phi - Nc\chi)\ = 0, \end{aligned} \tag{16}$$

$$\begin{aligned} &\left(1 + \tfrac{4}{3}Rd\right)\theta'' + \Pr\left(f\theta' + Nb\theta'\phi' + Nt(\theta')^2\right) + \delta\theta + \delta\lambda_T f\theta' \\ &+\Pr\lambda_T\begin{pmatrix} -ff'\theta' - f^2\theta'' - 2Ntf\theta'\theta'' \\ -Nbf\theta'\phi'' - Nbf\theta''\phi' \end{pmatrix} = 0, \end{aligned} \tag{17}$$

$$\begin{aligned} &\phi'' + Le\Pr f\phi' - Le\Pr\sigma^*(1 + \delta_0\theta)^n \exp\left(\tfrac{-E}{1+\delta_0\theta}\right)\phi - k_1\lambda_C f\phi' \\ &+Le\Pr\lambda_C\left[-ff'\phi' - f^2\phi'' - \tfrac{Nt}{Nb}\theta'''f + \tfrac{Nt}{Nb}\theta''\right] = 0, \end{aligned} \tag{18}$$

$$\chi'' + Lb\chi'f - Pe[\phi''(\chi + \delta) + \chi'\phi'] = 0, \tag{19}$$

$$\begin{aligned} &f = 0,\ f' = 1,\ \theta' = -\gamma_1(1 - \theta(\zeta)), \phi' = -\gamma_2(1 - \phi(\zeta)), \\ &\chi' = -\gamma_3(1 - \chi(\zeta))\ \ at\ \zeta = 0, \end{aligned} \tag{20}$$

$$f' \to K, f'' \to 0, \theta \to 0,\ \phi \to 0,\ \chi \to 0\ as\ \zeta \to \infty, \tag{21}$$

where $(\Pr)$ stands for the Prandtl number, (Nt) for the thermophoresis parameter, (λ_T) for the thermal relaxation parameter, (Nb) for the Brownian motion parameter, (Nc) for the bioconvection Rayleigh parameter, (Rd) for the thermal radiation parameter, (α_1, α_3) for the Deborah numbers, (α_2) for the Burgers' fluid parameter, (M) for the magnetic parameter, (Lb) for the bioconvection Lewis parameter, (Pe) for the Peclet parameter, (δ) for the microorganism difference number, (Le) for the Lewis number, (λ_C) for the mass relaxation parameter, (E) for the activation energy, (Nr) for the buoyancy ratio number, (δ_0) for the temperature difference parameter and (σ^*) for the chemical reaction parameter, which are defined as follows:

$$\left.Pe = \frac{bW_c}{D_m}, Lb = \frac{v}{D_m}, \delta = \frac{N_\infty}{N_w - N_0},\right\},$$

$$\left.\begin{aligned} &\Pr = \tfrac{v}{\alpha}, Nt = \tfrac{\tau D_T(T_w-T_\infty)}{vT_\infty}, \lambda_T = c\lambda^*t, Nb = \tfrac{\tau D_B(C_w-C_\infty)}{v}, \delta = \tfrac{vQ_0}{c(\rho c)f} \\ &Rd = \tfrac{4\sigma^*T_\infty^3}{k^*} \end{aligned}\right\},$$

$$\left.Le = \frac{\alpha}{D_B}, \lambda_C = a\lambda^*c,\ E = \frac{E_a}{kT_\infty}\delta_0 = \frac{T_w - T_0}{T_\infty}, \sigma^* = \frac{vKr^2}{a}\right\},$$

$$\left.\begin{array}{l}\alpha_1 = c\lambda_1, \alpha_2 = c\lambda_2, \beta_3 = c\lambda_3 \\ M = \left(\frac{\sigma l B_0^2}{\rho f U_0}\right)^{\frac{1}{2}}, \lambda\left(= \frac{(1-C_\infty)\gamma(T_w - T_0)\beta^{**}}{aU_w}\right), \\ Nr = \frac{(\rho_p - \rho_f)(C_w - C_o)}{(1-C_\infty)(T_w - T_0)}, Nc = \frac{\gamma g(\rho_m - \rho_f)(N_w - N_0)}{(1-C_\infty)(T_w - T_0)\beta^{**}}\end{array}\right\}, \tag{22}$$

3. Numerical Approach

Due to the accuracy and efficiency, the nonlinear ODEs (16)–(19) with boundary restrictions (20) and (21) are solved numerically by using the bvp4c solver in the MATLAB computational software. Fourth-order collocation method is described via the bvp4c technique. Furthermore, the Lobatto-IIIa relation is considered to have a tolerance factor of 10^{-7}. Initially the set of nonlinear ODEs are converted into a first order initial value problem. Let:

$$\left.\begin{array}{l} f = p_1, f' = p_2, f'' = p_3, f''' = p_4, f^{iv} = p'_4, \theta = p_5, \theta' = p_6, \\ \theta'' = p'_6, \phi = p_7, \phi' = p_8, , \phi'' = p'_8, \chi = p_9, \chi' = p_{10}, \chi'' = p'_{10} \end{array}\right\}, \tag{23}$$

$$p'_4, = \frac{\begin{array}{c} p_4 + p_1p_3 - (p_2)^2 + \alpha_1\left[2p_1p_2p_3 - p_1^2p_4\right] - \alpha_2\left[3p_1^2(p_3)^2 - 2p_1(p_2)^2p_3\right] \\ +\alpha_3\left[(p_3)^2\right] - M^2[\alpha_2p_1p_4 - \alpha_1p_1p_3 + p_2] + K^2 + M^2K + \lambda(p_5 - Nrp_8 - Ncp_9) \end{array}}{\left(\alpha_3p_1 - \alpha_2p_1^3\right)} \tag{24}$$

$$p'_6, = \frac{\Pr\left(p_1p_6 + Nbp_6p_8 + Nt(p_6)^2\right) + \delta p_5 + \delta\lambda_T p_1p_5 + \Pr\lambda_T\left(\begin{array}{c} -p_1p_2p_6 \\ -Nbp_1p_6p'_8 \end{array}\right)}{\left(\Pr\lambda_T f^2 + \Pr\lambda_T 2Ntp_1p_6 + \Pr\lambda_T Nbp_1p_8 - 1 - \frac{4}{3}Rd\right)} \tag{25}$$

$$\begin{array}{l} p'_8 = -Le\Pr p_1p_8 + Le\Pr\sigma^*(1 + \delta_0p_5)^n \exp\left(\frac{-E}{1+\delta_0p_5}\right)p_7 + k_1\lambda_C p_1p_8 \\ -Le\Pr\lambda_C\left[-p_1p_2p_8 - p_1^2, p'_8 - \frac{Nt}{Nb}p'_6p_1 + \frac{Nt}{Nb}p'_6\right], \end{array} \tag{26}$$

$$\chi'' = -Lbp_{10}p_1 + Pe\left[p'_8(p_9 + \delta) + p_9p_8\right] = 0, \tag{27}$$

with:

$$\begin{array}{l} p_1 = 0,\ p_2 = 1, p_8 = -\gamma_1(1 - p_7(\zeta)), p_8 = -\gamma_2(1 - p_7(\zeta)), \\ p_{10} = -\gamma_3(1 - p_9(\zeta)) \qquad at\ \zeta = 0, \end{array} \tag{28}$$

$$p_2 \to K, p_3 \to 0, p_5 \to 0,\ p_7 \to 0,\ p_9 \to 0 \quad as\ \zeta \to \infty. \tag{29}$$

4. Results and Discussion

In this segment, the physical significance of prominent parameters like thermophoresis parameter $Nt(0.1 \le Nt \le 2.2)$, magnetic parameter $M(0.1 \le M \le 1.2)$, Burgers fluid parameter $\alpha_2(0.1 \le \alpha_2 \le 2.2)$, Deborah number $\alpha_1(0.1 \le \alpha_1 \le 1.5)$, bioconvection Rayleigh number $Nc(0.1 \le Nc \le 2.2)$, Deborah number $\alpha_3(0.1 \le \alpha_3 \le 2.2)$, buoyancy ratio parameter $Nr(0.1 \le Nr \le 2.0)$, velocity ratio parameter $K(0.2 \le K \le 1.6)$, mixed convection parameter $\lambda(0.1 \le \lambda \le 2.2)$, thermal relaxation parameter $\lambda_T(0.1 \le \lambda_T \le 2.2)$, thermal Biot number $\gamma_1(0.1 \le \gamma_1 \le 1.0)$, Prandtl number $Pr(2.0 \le Pr \le 5.0)$, activation energy parameter $E(0.1 \le E \le 2.0)$, solutal Biot number $\gamma_2(0.1 \le \gamma_2 \le 1.6)$, thermal radiation number $Rd(0.1 \le Rd \le 1.6)$, Brownian motion number $Nb(0.1 \le Nb \le 0.8)$, Lewis parameter $Le(1.2 \le Le \le 2.4)$, microorganism Biot number $\gamma_3(0.1 \le \gamma_3 \le 1.6)$, Peclet number $Pe(0.1 \le Pe \le 1.2)$ and bioconvection Lewis number $Lb(1.0 \le Lb \le 3.0)$ against velocity, temperature, volumetric concentration of nanoparticles and motile microorganisms is deliberated through Figures 2–15. Figure 2 represents the performance of velocity field f' for growing magnetic parameter M and Burgers' parameter α_2. Clearly the velocity of fluid f' reduces for growing estimations of the magnetic number M and the Burgers' parameter α_2. This scenario is observed for different values of both numbers. By raising the magnetic number, a resistive force is developed, which causes decay in the motion of the Burgers' nanofluid. The aspects of the Deborah number α_1 and bioconvection Rayleigh number Nc

versus velocity flow field f' are plotted in Figure 3. Reduction is observed in the velocity of the Burgers' nanofluid f' due to the increased values of the Deborah number α_1. Furthermore, it is analyzed that the decay of velocity f' is due to rises in the bioconvection Rayleigh parameter Nc. Features of the velocity f' due to the Deborah number for retardation α_3 and the buoyancy ratio parameter Nr are exhibited in Figure 4. The velocity of the Burgers' nanofluid f' increases for a larger Deborah number for retardation time parameter α_3. It is also depicted that the velocity field f' diminishes with a higher amount of the buoyancy ratio number Nr. The performance of the velocity ratio number K and mixed convection parameter λ against the velocity f' is plotted in Figure 5. Here the velocity of Burgers' nanofluid f' is enhanced by increasing the values of the velocity ratio parameter K and mixed convective number λ. The consequences of the thermal relaxation number λ_T and Burgers' number α_2 changes over temperature field θ are examined in Figure 6. An increment in the thermal relaxation parameter λ_T corresponds to a weaker temperature field θ. It is also noted that the temperature field θ upsurges for a higher magnitude of the Burgers' parameter α_2. The thermal relaxation parameter is directly proportional to the thermal relaxation time. A greater thermal relaxation parameter indicates a higher relaxation time which produces a weaker temperature field. Figure 7 depicts the effects of the thermal Biot number γ_1 and thermophoresis parameter Nt versus the temperature field θ. It is noted that the temperature field θ upsurges with a larger thermal Biot number γ_1. Here it is also witnessed that the temperature field θ augments with rising variation of the thermophoresis number Nt. A growing thermophoresis number depicts a stronger thermophoretic force which produces a stronger temperature field. Figure 8 shows the physical appearance of the Prandtl number Pr and the thermal radiation parameter Rd against the temperature field θ. It can be verified that the temperature distribution θ is retarded by varying the Prandtl number Pr. Here, it is also noted that the temperature θ is increased with higher estimations of the thermal radiation parameter Rd. Figure 9 examines the variation in nanoparticles concentration ϕ for different estimations of the thermophoresis parameter Nt and the activation energy parameter E. It is noted that the volumetric concentration of nanoparticles ϕ is upgraded by increasing the estimations of the thermophoresis parameter Nt. It is also analyzed that the volumetric concentration of nanoparticles ϕ is enlarged with larger estimations of the activation energy parameter E. Figure 10 elucidates the behavior of the solutal Biot number γ_2 and the buoyancy ratio parameter Nr with the concentration of nanoparticles ϕ. Here the concentration of nanoparticles ϕ is enhanced for a larger solutal Biot number γ_2 and the buoyancy ratio parameter Nr. Features of the effect of the Brownian motion number Nb and Burgers' number α_2 on the volumetric concentration of nanoparticles ϕ are plotted in Figure 11. It is illustrated that the nanoparticles concentration ϕ is decayed with a larger Brownian motion number Nb. It is also analyzed that the concentration field ϕ is knocked down due to the Burgers' parameter α_2. Brownian motion develops due to the occurrence of nanoparticles and results in the decay of the nanoparticle concentration thickness. The characteristics of the Prandtl number Pr and Lewis number versus volumetric concentration of nanoparticles ϕ are shown in Figure 12. It is observed that the concentration field ϕ diminishes for a higher Prandtl number Pr and Lewis number Le. The Lewis number is inversely proportional to the Brownian diffusivity. A greater Lewis number indicates a lower Brownian diffusivity which produces a weaker nanoparticles concentration field. Figure 13 shows the microorganism's field χ for various values of the Burgers' parameter α_2 and the buoyancy ratio parameter Nr. An increment in the Burgers' parameter α_2 and buoyancy ratio parameter Nr leads to a stronger microorganism profile χ. Figure 14 displays the characteristics of the microorganism Biot number γ_3 and bioconvection Rayleigh number Nc against the swimming motile microorganism profile χ. The swimming motile microorganism field χ is increased as the enlarging microorganism Biot number γ_3 and bioconvection Rayleigh number Nc increase. The outcomes of the microorganism profile χ versus Peclet Pe and bioconvection Lewis Lb parameters are shown in Figure 15. The swimming motile microorganism field χ declines with the Peclet number Pe and the bioconvection Lewis number Lb. From Table 1, it can be noted that the skin friction coefficient $-f''(0)$ increases for M and Nr. From Table 2, it can be concluded that the local Nusselt number $-\theta'(0)$ declines with growing variations of Nb and Rd. From Table 3, it is analyzed that the local Sherwood number $-\phi'(0)$ increases with K. The microorganism density number $-\chi'(0)$ reduces for Pe while it is enhanced with growing estimations of γ_3 (see Table 4). Table 5 is constructed to validate the presented numerical solution with previously determined solution in a limiting situation. It is witnessed that the presented numerical solution shows good agreement with the solution previous reported by Iqbal et al. [30] in a limiting situation.

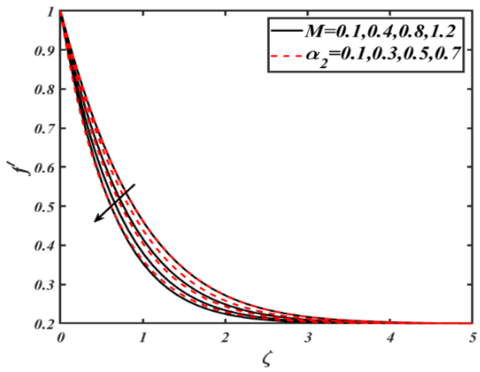

Figure 2. Performance of M and α_2 versus f'.

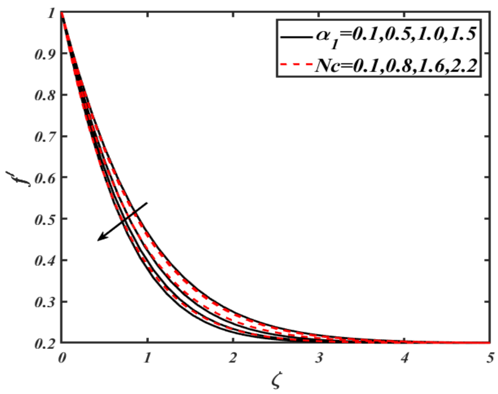

Figure 3. Performance of α_1 and Nc versus f'.

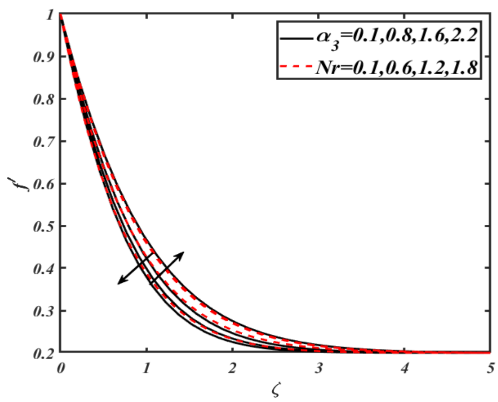

Figure 4. Performance of α_3 and Nr versus f'.

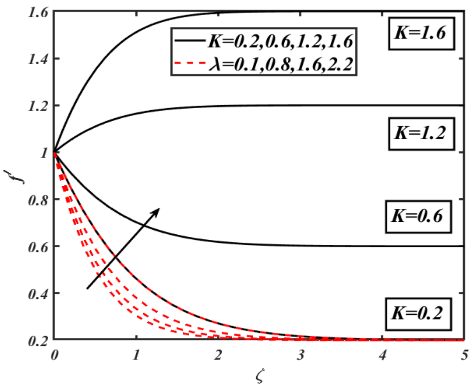

Figure 5. Performance of K and λ versus f'.

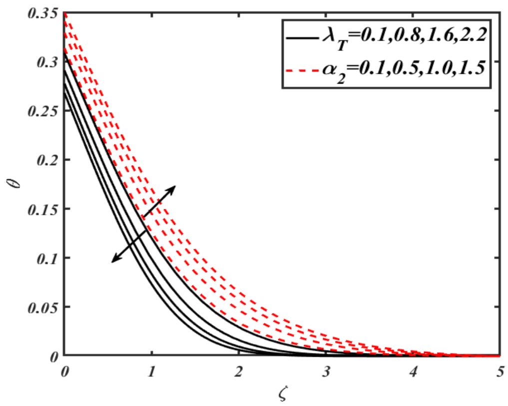

Figure 6. Performance of λ_T and α_2 versus θ.

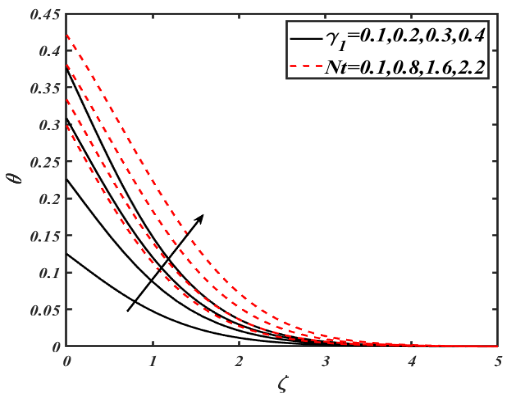

Figure 7. Performance of γ_1 and Nt versus θ.

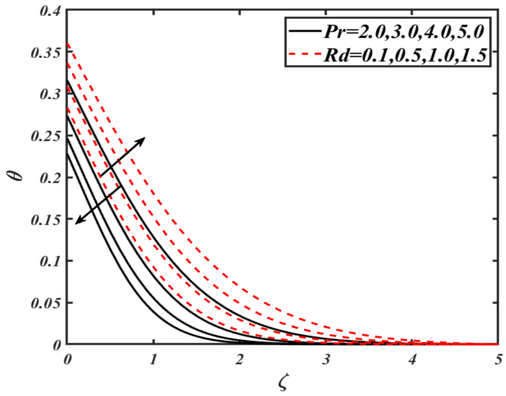

Figure 8. Performance of Pr and Rd versus θ.

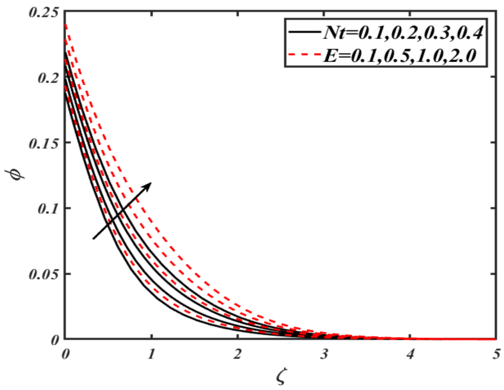

Figure 9. Performance of Nt and E versus ϕ.

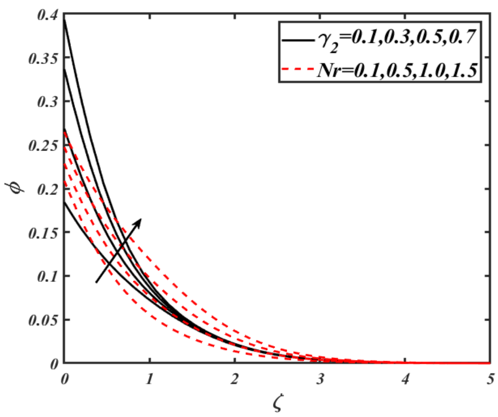

Figure 10. Performance of γ_2 and Nr versus ϕ.

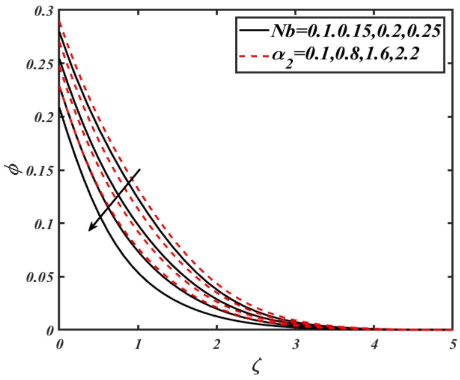

Figure 11. Performance of Nb and α_2 versus ϕ.

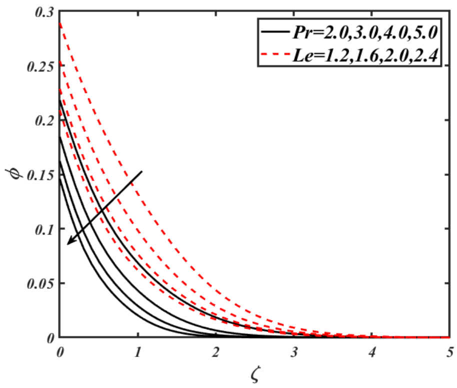

Figure 12. Performance of Pr and Le versus ϕ.

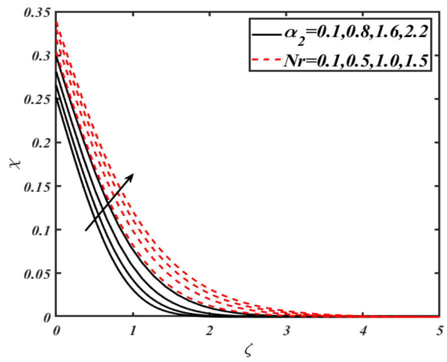

Figure 13. Performance of α_2 and Nr versus χ.

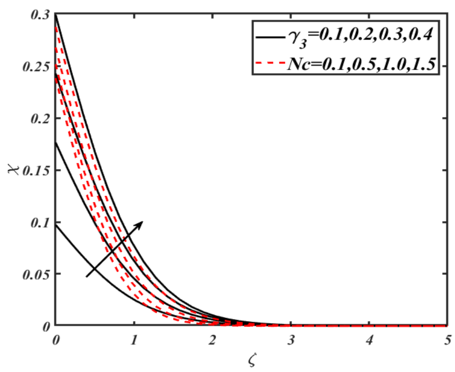

Figure 14. Performance of γ_3 and Nc versus χ.

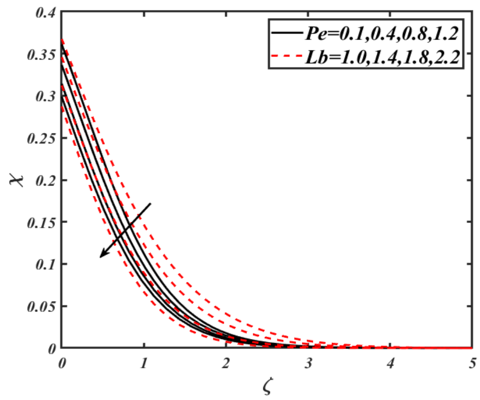

Figure 15. Performance of Pe and Lb versus χ.

Table 1. Variations of $-f''(0)$ for M, K, λ, Nr, Nc, α_1, α_2 *and* α_3.

M	K	λ	Nr	Nc	α_1	α_2	α_3	$-f''(0)$
0.1 0.5 1.0	0.1	0.1	0.1	0.1	0.2	0.2	0.2	0.2867 0.9398 1.0320
0.4	0.2 0.5 0.8	0.1	0.1	0.1	0.2	0.2	0.2	0.8569 0.6030 0.2641
0.4	0.1	0.2 0.8 1.6	0.1	0.1	0.2	0.2	0.2	0.9142 0.8803 0.8365
0.4	0.1	0.1	0.2 1.0 2.0	0.1	0.2	0.2	0.2	0.9203 0.9239 0.9284
0.4	0.1	0.1	0.1	0.2 1.0 2.0	0.2	0.2	0.2	0.9204 0.9242 0.9291
0.4	0.1	0.1	0.1	0.1	0.1 0.5 1.0	0.2	0.2	0.9158 0.9112 0.9591
0.4	0.1	0.1	0.1	0.1	0.2	0.1 0.5 1.0	0.2	0.9090 0.9506 0.9991
0.4	0.1	0.1	0.1	0.1	0.2	0.2	0.1 0.5 1.0	0.9463 0.9112 0.8681

Table 2. Variations of $-\theta'(0)$ for M, K, Nb, Nt γ_1.

M	K	Nb	Nt	Rd	γ_1	$-\theta'(0)$
0.1						0.2060
0.5	0.1	0.3	0.2	0.4	0.3	0.2048
1.0						0.2035
	0.2					0.2068
0.4	0.5	0.3	0.2	0.4	0.3	0.2114
	0.8					0.2149
		0.1				0.2059
0.4	0.1	0.4	0.2	0.4	0.3	0.2026
		0.8				0.1982
			0.1			0.2078
0.4	0.1	0.3	0.4	0.4	0.3	0.2033
			0.8			0.1968
				0.1		0.3130
0.4	0.1	0.3	0.2	0.8	0.3	0.1961
				1.6		0.1824
					0.1	0.0871
0.4	0.1	0.3	0.2	0.4	0.5	0.2791
					1.0	0.3787

Table 3. Variations of $-\phi'(0)$ for M, K, Nb, Nt γ_2.

M	K	Nb	Nt	Rd	γ_2	$-\phi'(0)$
0.1						0.2303
0.5	0.1	0.3	0.2	0.4	0.3	0.2295
1.0						0.2287
	0.2					0.2310
0.4	0.5	0.3	0.2	0.4	0.3	0.2377
	0.8					0.2346
		0.1				0.2087
0.4	0.1	0.4	0.2	0.4	0.3	0.2399
		0.8				0.2451
			0.1			0.2424
0.4	0.1	0.3	0.4	0.4	0.3	0.2236
			0.8			0.2033
				0.1		0.2278
0.4	0.1	0.3	0.2	0.8	0.3	0.2316
				1.6		0.2346
					0.1	0.0860
0.4	0.1	0.3	0.2	0.4	0.8	0.4802
					1.6	0.7137

Table 4. Variations of $-\chi'(0)$ for M, K, λ, Nr, γ_3, γ_3, *Pe and Lb*.

M	K	λ	Nr	γ_3	Pe	Lb	$-\chi'(0)$
0.1							0.2786
0.5	0.1	0.1	0.1	0.3	0.1	0.1	0.2771
1.0							0.2755
	0.2						0.2796
0.4	0.5	0.1	0.1	0.3	0.1	0.1	0.2855
	0.8						0.2907
		0.2					0.2776
0.4	0.1	0.8	0.1	0.3	0.1	0.1	0.2781
		1.6					0.2788
			0.2				0.2775
0.4	0.1	0.1	1.0	0.3	0.1	0.1	0.2774
			2.0				0.2773
				0.1			0.0900
0.4	0.1	0.1	0.1	0.8	0.1	0.1	0.4251
				1.6			0.5793
					0.2		0.2757
0.4	0.1	0.1	0.1	0.3	0.5	0.1	0.2565
					1.0		0.2265
						1.0	0.2373
0.4	0.1	0.1	0.1	0.3	0.1	2.0	0.2973
						3.0	0.3184

Table 5. Comparative outcomes of $-\theta'(0)$ for various estimations of Pr when $\lambda = Nr = Nc = E = Le = Lb = 0$.

Pr	Iqbal et al. [30]	Present Results
0.7	0.45312	0.45312
2.0	0.90894	0.90894
7.0	1.88986	1.88985

5. Conclusions

The effects of bio-convection and motile microorganisms in a magnetized Burgers' nanofluid flow due to a stretching sheet are studied. Cattaneo–Christov double diffusion theory is also discussed. The Buongiorno phenomenon for nanoparticles motion in a Burgers' fluid is employed in view of the Cattaneo–Christov relations. The velocity field of a Burgers' nanofluid is a diminishing function of the Burgers' fluid parameters. The velocity field of a Burgers' nanofluid decays for buoyancy ratio and bioconvection Rayleigh numbers while it is enhanced for a mixed convective number. A reduction in temperature is analyzed for growing estimations of the thermal relaxation parameter. An increment in the thermal Biot, thermophoresis and radiation parameters leads to a stronger temperature field. Nanoparticles concentration is reduced for growing Brownian motion and Lewis numbers. The microorganism profile is enhanced by growing estimations of the microorganism Biot and bioconvection Rayleigh numbers. The microorganism field is reduced by increasing estimations of the Peclet and bioconvection Lewis numbers.

Funding: This research was funded by the Deanship of Scientific Research (DSR), King Abdulaziz University, Jeddah, Saudi Arabia under grant No. (D-035-130-1437).

Acknowledgments: This work was supported by the Deanship of Scientific Research (DSR), King Abdulaziz University, Jeddah, under grant No. (D-035-130-1437). The author, therefore, gratefully acknowledge the DSR technical and financial support.

Conflicts of Interest: The author declares no conflict of interest.

References

1. Choi, S.U.S. *Enhancing Thermal Conductivity of Fluids with Nanoparticles*; FED 231/MD; ASME: New York, NY, USA, 1995; pp. 99–105.
2. Buongiorno, J. Convective transport in nanofluids. *ASME J. Heat Transf.* **2006**, *128*, 240–250. [CrossRef]
3. Turkyilmazoglu, M. Single phase nanofluids in fluid mechanics and their hydrodynamic linear stability analysis. *Comput. Methods Programs Biomed.* **2020**, *187*, 105171. [CrossRef]
4. Ellahi, R.; Hussain, F.; Abbas, S.A.; Sarafraz, M.M.; Goodarzi, M.; Shadloo, M.S. Study of two-phase Newtonian nanofluid flow hybrid with Hafnium particles under the effects of slip. *Inventions* **2020**, *5*, 6. [CrossRef]
5. Alamri, S.Z.; Ellahi, R.; Shehzad, N.; Zeeshan, A. Convective radiative plane Poiseuille flow of nanofluid through porous medium with slip: An application of Stefan blowing. *J. Mol. Liq.* **2019**, *273*, 292–304. [CrossRef]
6. Khan, A.M.; Jamil, M.; Mia, M.; He, N.; Zhao, W.; Gong, L. Sustainability-based performance evaluation of hybrid nanofluid assisted machining. *J. Clean. Prod.* **2020**, *257*, 120541. [CrossRef]
7. Irfan, M.; Farooq, M.A.; Iqra, T. A new computational technique design for EMHD nanofluid flow over a variable thickness surface with variable liquid characteristics. *Front. Phys.* **2020**, *8*, 66. [CrossRef]
8. Reddy, S.R.R.; Reddy, P.B.A.; Rashad, A.M. Activation energy impact on chemically reacting Eyring–Powell nanofluid flow over a stretching cylinder. *Arab. J. Sci. Eng.* **2020**, *45*, 5227–5242. [CrossRef]
9. Khan, S.U.; Tlili, I.; Waqas, H.; Imran, M. Effects of nonlinear thermal radiation and activation energy on modified second-grade nanofluid with Cattaneo-Christov expressions. *J. Therm. Anal. Calorim.* **2020**. [CrossRef]
10. Alghamdi, M. On magnetohydrodynamic flow of viscoelastic nanofluids with homogeneous-heterogeneous reactions. *Coatings* **2020**, *10*, 55. [CrossRef]
11. Uddin, S.; Mohamad, M.; Rahimi-Gorji, M.; Roslan, R.; Alarifi, I.M. Fractional electro-magneto transport of blood modeled with magnetic particles in cylindrical tube without singular kernel. *Microsyst. Technol.* **2020**, *26*, 405–414. [CrossRef]
12. Abbas, M.A.; Bhatti, M.M.; Sheikholeslami, M. Peristaltic propulsion of Jeffrey nanofluid with thermal radiation and chemical reaction effects. *Inventions* **2019**, *4*, 68. [CrossRef]
13. Babazadeh, H.; Muhammad, T.; Shakeriaski, F.; Ramzan, M.; Hajizadeh, M.R. Nanomaterial between two plates which are squeezed with impose magnetic force. *J. Therm. Anal. Calorim.* **2020**. [CrossRef]
14. Balankin, A.S.; Golmankhaneh, A.K.; Patiño-Ortiz, J.; Patiño-Ortiz, M. Noteworthy fractal features and transport properties of Cantor tartans. *Phys. Lett. A* **2018**, *382*, 1534–1539. [CrossRef]
15. Niazmand, A.; Sola, J.F.; Alinejad, F.; Dehgolan, F.R. Investigation of mixed convection in a cylindrical lid driven cavity filled with water-Cu nanofluid. *Inventions* **2019**, *4*, 60. [CrossRef]
16. Mondal, H.; Das, S.; Kundu, P.K. Influence of an inclined stretching cylinder over MHD mixed convective nanofluid flow due to chemical reaction and viscous dissipation. *Heat Transf.* **2020**, *49*, 2183–2193. [CrossRef]
17. Bhatti, M.M.; Michaelides, E.E. Study of Arrhenius activation energy on the thermo-bioconvection nanofluid flow over a Riga plate. *J. Therm. Anal. Calorim.* **2020**. [CrossRef]
18. Abdulrazzaq, T.; Togun, H.; Goodarzi, M.; Kazi, S.N.; Ariffin, M.K.A.; Adam, N.M.; Hooman, K. Turbulent heat transfer and nanofluid flow in an annular cylinder with sudden reduction. *J. Therm. Anal. Calorim.* **2020**, *141*, 373–385. [CrossRef]
19. Saeed, A.; Tassaddiq, A.; Khan, A.; Jawad, M.; Deebani, W.; Shah, Z.; Islam, S. Darcy-Forchheimer MHD hybrid nanofluid flow and heat transfer analysis over a porous stretching cylinder. *Coatings* **2020**, *10*, 391. [CrossRef]
20. Souayeh, B.; Kumar, K.G.; Reddy, M.G.; Rani, S.; Hdhiri, N.; Alfannakh, H.; Rahimi-Gorji, M. Slip flow and radiative heat transfer behavior of Titanium alloy and ferromagnetic nanoparticles along with suspension of dusty fluid. *J. Mol. Liq.* **2019**, *290*, 111223. [CrossRef]
21. Tlili, I.; Hamadneh, N.N.; Khan, W.A. Thermodynamic analysis of MHD heat and mass transfer of nanofluids past a static wedge with Navier slip and convective boundary conditions. *Arab. J. Sci. Eng.* **2019**, *44*, 1255–1267. [CrossRef]

22. Farhangmehr, V.; Moghadasi, H.; Asiaei, S. A nanofluid MHD flow with heat and mass transfers over a sheet by nonlinear boundary conditions: Heat and mass transfers enhancement. *J. Cent. South Univ.* **2019**, *26*, 1205–1217. [CrossRef]
23. Khan, M.; Irfan, M.; Khan, W.A. Impact of nonlinear thermal radiation and gyrotactic microorganisms on the Magneto-Burgers nanofluid. *Int. J. Mech. Sci.* **2017**, *130*, 375–382. [CrossRef]
24. Khan, M.; Khan, W.A.; Alshomrani, A.S. Non-linear radiative flow of three-dimensional Burgers nanofluid with new mass flux effect. *Int. J. Heat Mass Transf.* **2016**, *101*, 570–576. [CrossRef]
25. Khan, M.; Khan, W.A. Forced convection analysis for generalized Burgers nanofluid flow over a stretching sheet. *AIP Adv.* **2015**, *5*, 107138. [CrossRef]
26. Hayat, T.; Waqas, M.; Shehzad, S.A.; Alsaedi, A. Mixed convection flow of a Burgers nanofluid in the presence of stratifications and heat generation/absorption. *Eur. Phys. J. Plus* **2016**, *131*, 253. [CrossRef]
27. Hayat, T.; Aziz, A.; Muhammad, T.; Alsaedi, A. On model for flow of Burgers nanofluid with Cattaneo—Christov double diffusion. *Chin. J. Phys.* **2017**, *55*, 916–929. [CrossRef]
28. Hayat, T.; Waqas, M.; Shehzad, S.A.; Alsaedi, A. On model of Burgers fluid subject to magneto nanoparticles and convective conditions. *J. Mol. Liq.* **2016**, *222*, 181–187. [CrossRef]
29. Rashidi, M.M.; Yang, Z.; Awais, M.; Nawaz, M.; Hayat, T. Generalized magnetic field effects in Burgers' nanofluid model. *PLoS ONE* **2017**, *12*, e0168923. [CrossRef]
30. Iqbal, Z.; Khan, M.; Ahmed, J.; Hafeez, A. Thermal energy transport in Burgers nanofluid flow featuring the Cattaneo-Christov double diffusion theory. *Appl. Nanosci.* **2020**. [CrossRef]
31. Kuznetsov, A.V.; Avramenko, A.A. Effect of small particles on this stability of bioconvection in a suspension of gyrotactic microorganisms in a layer of finite depth. *Int. Commun. Heat Mass Transf.* **2004**, *31*, 1–10. [CrossRef]
32. Ghorai, S.; Hill, N.A. Wavelengths of gyrotactic plumes in bioconvection. *Bull. Math. Biol.* **2000**, *62*, 429–450. [CrossRef] [PubMed]
33. Atif, S.M.; Hussain, S.; Sagheer, M. Magnetohydrodynamic stratified bioconvective flow of micropolar nanofluid due to gyrotactic microorganisms. *AIP Adv.* **2019**, *9*, 025208. [CrossRef]
34. Khan, S.U.; Waqas, H.; Bhatti, M.M.; Imran, M. Bioconvection in the rheology of magnetized couple stress nanofluid featuring activation energy and Wu's slip. *J. Non Equilib. Thermodyn.* **2020**, *45*, 81–95. [CrossRef]
35. Amirsom, N.A.; Uddin, M.J.; Basir, M.F.M.; Ismail, A.I.M.; Beg, O.A.; Kadir, A. Three-dimensional bioconvection nanofluid flow from a bi-axial stretching sheet with anisotropic slip. *Sains Malays.* **2019**, *48*, 1137–1149. [CrossRef]
36. Zhang, T.; Khan, S.U.; Imran, M.; Tlili, I.; Waqas, H.; Ali, N. Activation energy and thermal radiation aspects in bioconvection flow of rate-type nanoparticles configured by a stretching/shrinking disk. *J. Energy Resour. Technol.* **2020**, *142*, 112102. [CrossRef]
37. Usman, M.; Hamid, M.; Rashidi, M.M. Gegenbauer wavelets collocation-based scheme to explore the solution of free bio-convection of nanofluid in 3D nearby stagnation point. *Neural Comput. Appl.* **2019**, *31*, 8003–8019. [CrossRef]
38. Basir, M.F.M.; Uddin, M.J.; Ismail, A.I.M. Scaling group analysis of mixed bioconvective flow in nanofluid with presence of slips, MHD and chemical reactions. *Preprints* **2018**. [CrossRef]
39. Muhammad, T.; Alamri, S.Z.; Waqas, H.; Habib, D.; Ellahi, R. Bioconvection flow of magnetized Carreau nanofluid under the influence of slip over a wedge with motile microorganisms. *J. Therm. Anal. Calorim.* **2020**. [CrossRef]
40. Mansour, M.A.; Rashad, A.M.; Mallikarjuna, B.; Hussein, A.K.; Aichouni, M.; Kolsi, L. MHD mixed bioconvection in a square porous cavity filled by gyrotactic microorganisms. *Int. J. Heat Technol.* **2019**, *37*, 433–445. [CrossRef]
41. Li, Y.; Waqas, H.; Imran, M.; Farooq, U.; Mallawi, F.; Tlili, I. A numerical exploration of modified second-grade nanofluid with motile microorganisms, thermal radiation, and Wu's slip. *Symmetry* **2020**, *12*, 393. [CrossRef]
42. Waqas, H.; Imran, M.; Muhammad, T.; Sait, S.M.; Ellahi, R. Numerical investigation on bioconvection flow of Oldroyd B nanofluid with nonlinear thermal radiation and motile microorganisms over rotating disk. *J. Therm. Anal. Calorim.* **2020**. [CrossRef]
43. Waqas, H.; Khan, S.U.; Imran, M.; Bhatti, M.M. Thermally developed Falkner-Skan bioconvection flow of a magnetized nanofluid in the presence of a motile gyrotactic microorganism: Buongiorno's nanofluid model. *Phys. Scr.* **2019**, *94*, 115304. [CrossRef]

44. Alwatban, A.M.; Khan, S.U.; Waqas, H.; Tlili, I. Interaction of Wu's slip features in bioconvection of Eyring Powell nanoparticles with activation energy. *Processes* **2019**, *7*, 859. [CrossRef]
45. Waqas, H.; Khan, S.U.; Hassan, M.; Bhatti, M.M.; Imran, M. Analysis on the bioconvection flow of modified second-grade nanofluid containing gyrotactic microorganisms and nanoparticles. *J. Mol. Liq.* **2019**, *291*, 111231. [CrossRef]
46. Waqas, H.; Shehzad, S.A.; Khan, S.U.; Imran, M. Novel numerical computations on flow of nanoparticles in porous rotating disk with multiple slip effects and microorganisms. *J. Nanofluids* **2019**, *8*, 1423–1432. [CrossRef]
47. Wang, Y.; Waqas, H.; Tahir, M.; Imran, M.; Jung, C.Y. Effective Prandtl aspects on bio-convective thermally developed magnetized tangent hyperbolic nanoliquid with gyrotactic microorganisms and second order velocity slip. *IEEE Access* **2019**, *7*, 130008–130023. [CrossRef]
48. Tlili, I.; Waqas, H.; Almaneea, A.; Khan, S.U.; Imran, M. Activation energy and second order slip in bioconvection of Oldroyd-B nanofluid over a stretching cylinder: A proposed mathematical model. *Processes* **2019**, *7*, 914. [CrossRef]
49. Ullah, M.Z.; Jang, T.S. An efficient numerical scheme for analyzing bioconvection in von-Kármán flow of third-grade nanofluid with motile microorganisms. *Alex. Eng. J.* **2020**. [CrossRef]
50. Shahid, A.; Huang, H.; Bhatti, M.M.; Zhang, L.; Ellahi, R. Numerical investigation on the swimming of gyrotactic microorganisms in nanofluids through porous medium over a stretched surface. *Mathematics* **2020**, *8*, 380. [CrossRef]
51. Asma, M.; Othman, W.A.M.; Muhammad, T. Numerical study for Darcy-Forchheimer flow of nanofluid due to a rotating disk with binary chemical reaction and Arrhenius activation energy. *Mathematics* **2019**, *7*, 921. [CrossRef]
52. Zhu, J.; Xu, Y.; Han, X. A non-Newtonian magnetohydrodynamics (MHD) nanofluid flow and heat transfer with nonlinear slip and temperature jump. *Mathematics* **2019**, *7*, 1199. [CrossRef]
53. Waini, I.; Ishak, A.; Pop, I. Hybrid nanofluid flow past a permeable moving thin needle. *Mathematics* **2020**, *8*, 612. [CrossRef]
54. Waini, I.; Ishak, A.; Pop, I. Squeezed hybrid nanofluid flow over a permeable sensor surface. *Mathematics* **2020**, *8*, 898. [CrossRef]